Automotive Experiences
Vol. 7 No. 1 (2024) pp. 28-47
p-ISSN: 2615-6202 e-ISSN: 2615-6636

Research Paper

Application of Multi-objective Adjoint-based Aerodynamic Optimisation on Generic Road Vehicle with Rear Spoiler

Aan Yudianto

Department of Automotive and Mechanical Engineering, Universitas Negeri Yogyakarta, 55281, Indonesia

aan.yudianto@uny.ac.id

https://doi.org/10.31603/ae.10577

Published by Automotive Laboratory of Universitas Muhammadiyah Magelang

Article Info
Submitted:
21/11/2023
Revised:
27/03/2024
Accepted:
28/03/2024
Online first:
27/04/2024

Abstract

Finding possible solutions where there are multiple conflicting objectives to be simultaneously satisfied is a challenging situation. Multi-objective optimisation of a rear spoiler on a generic road vehicle model is carried out by using adjoint-based optimisation coupled with Computational Fluid Dynamics. The study aims to reduce the vehicle drag and increase vehicle downforce simultaneously by optimising the shape of the spoiler, by allowing the deformation to achieve the most optimised shape assuming no manufacturing constraint. The OpenFOAM software was used for the solver. A strategy for multi-objective optimisation was proposed by assigning appropriate objective function weight, leading to some possible solutions and Pareto front of the proposed design family. Five optimisation solutions of the non-dominated solution Pareto front resulting from the spoiler shape optimisation are presented, explaining the trade-off between conflicting drag and downforce objectives on the vehicle model. The baseline geometry of the simulation is in good agreement with the experimental measurement. The analysis of the shape changes in the proposed optimisation is deeply investigated in terms of the optimised geometry deformation, velocity contour comparison, recirculating region on the base, pressure coefficient comparison and stream-wise velocity component at the slant region of the model. The adjoint-based optimisation method in the presence study can handle multiple objective optimisations and generate possible optimised spoiler shapes to reduce drag and increase downforce. Free deformation of the shape yields in the unique shapes of the spoiler, enabling to manipulate of the base flow at the rear of the vehicle model.

Keywords: Adjoint; Multi-objective optimization; Ahmed body; Spoiler; Aerodynamics

1. Introduction

The application of computational methods for aerodynamic shape optimisation has gained research attention in many engineering fields, especially in the aeronautics [1], [2] and automotive field [3], [4]. Shape optimisation in road vehicle applications is generally aimed at reducing the aerodynamic drag [5], [6], increasing the downforce [7], [8], or reducing the side force due to the presence of crosswind [9], [10]. Reducing vehicle drag is more generally applied in almost all aerodynamic optimisations. The improvement of downforce is usually used for high-performance vehicles where handling at high speed is of interest, and the optimisation of the side force due to crosswind [10], [11] is mainly becoming one of the concerns for large vehicles such as tractor-trailer, train, bus, or lorry.

A road vehicle generally has a blunted body shape. The generated aerodynamic force is mainly caused by pressure components, and the skin friction force becomes less concerned. Therefore, attempts to improve a car's aerodynamic performance are primarily performed by suppressing or delaying separation on the vehicle body and controlling the structures at the rear of the vehicle body [12]. This base drag reduction can be done by applying passive aerodynamic devices

to improve the aerodynamic properties, which can be a general simple or sophisticated form, such as flaps [13], vortex generator [14], arrays of circular cylinder [15], rounder edge [16], blowing at the base [17], base cavity [18], boat tail [18] and rear spoiler [12]. Among the mentioned aerodynamic devices, the rear spoiler is one of the most used in road vehicle applications.

The definition of a rear spoiler for road vehicles is an aerodynamic device attached to the trailing edge of the vehicle trunk or roof to improve the aerodynamic performance [12]. The main aim of attaching this device is to improve the vehicle downforce, which usually conflicts with generating more drag values. Generating downforce in a vehicle enhances driving stability and safety since it is proportional to vehicle traction. Having more downforce in a vehicle also means better cornering performance since the downforce generates more traction, preventing a vehicle from slipping to some points.

One of the breakthroughs in the aerodynamic optimisation method is the application of adjoint-based optimisation. It has been recognised to be efficient in optimisation with many variables [3], [19]. The adjoint formulation allows for calculating the derivatives of the objective function with respect to design variables, which is called sensitivity. Another advantage of adjoint-based optimisation is that this method is independent of the number of variables. It only involves the Navier-Stokes equation and the adjoint solver. Considering the mentioned advantages, this method has been effectively applied in road vehicle aerodynamics. Some of the other available methods for shape aerodynamics can be seen in Ref [2].

Some research has utilised the adjoint method for optimisation for both internal and external aerodynamics. The implementation of adjoint method for internal aerodynamic optimisation was implemented in some geometries, such as the optimisation of the intake system geometry [20], a design of exhaust system [21], engine intake component [22]. The general objective for the internal aerodynamic problems is generally a reduction of total pressure loss, flow uniformity, or tumble moment improvement. However, the application of adjoint optimisation for external aerodynamics in the automotive field generally targets drag reduction or minimises side force due to crosswind. Some examples are drag reduction on the DrivAer geometry Field [23], which optimises the geometry's rear end shape to become spoiler-like after the optimisation. Multi-objective optimisation has also been performed to optimise both the spoiler and diffuser of a complex-shaped concept car to reduce both drag and side force moment coefficient due to crosswind [23]. The adjoint method can also be used for noise reduction due to the external aerodynamics of the side mirror car component [24].

Both generic model [10], [25] and realistic model [11], [26], [27] have been used for external automotive aerodynamic investigation. The generic simplification model was more commonly used due to the simplification reason, standardisation, and ease of benchmarking and comparison, and also for the sake of validation of the computational model. The present study uses the generic vehicle model Ahmed Body [28] with some modifications of the attachment of the rear spoiler. When dealing with the shape of the rear spoiler of a vehicle, the most proper shape depends on the flow history of the body to which the spoiler is attached. It leads to the current lack of understanding of the optimum shape of a rear spoiler of a vehicle for a generic body shape, which should be understood prior to the implementation of a more complex shape of a body. Addressing this research gap is vital for enabling deeper understanding of how small changes in a shape can affect the base drag of a vehicle by giving the shape to deform freely, without a restriction of manufacturing constraint, for the sake of the understanding of the optimised airflow over a body, which is essential at the initial design stages.

Additionally, satisfying optimisation objective in real-world problem can be challenging when there is more than one objective need to be satisfied. It is considered a more complex optimisation problem where the goal is to find the best possible solution with multiple conflicting objectives present. Those conflicting objectives are necessary to be satisfied simultaneously, such as reducing vehicle drag while also it is necessary to increase downforce. Here, the main problem refers to a situation where it is necessary to find a set of solutions that balance multiple, or often competing criteria. Therefore, this study aims to

develop an optimisation strategy to increase downforce and reduce the drag of a generic vehicle model with a spoiler. The main part of the model to be optimised is the spoiler attached to the rear end of the generic vehicle body trunk. Optimising vehicle's drag and improving vehicle downforce have potentially significant impacts on fuel efficiency and emission reduction for gasoline engines and increase the range of electric vehicles, enhancing vehicle handling and stability and leading to safer driving conditions.

2. Model Geometry, Mesh Setting and Boundary Conditions

This multi-objective optimisation considers the geometry of Ahmed body [28] without a stilt. The representation of Ahmed body in isometric and side view is shown in **Figure 1**. The dimension of the geometry is shown in **Figure 2**. The Dimension of the model, together with the spoiler is available in **Figure 2** as well. During the discussion, the so-called front, roof, spoiler, slant, base, and underbody definition is also explained. The geometry used in this simulation follows the geometry that has already been experimentally investigated by Cheng et al., which can be further checked in Ref [12]. The model, which in this article is also called the body, has a length (L) of 783 mm, height (H) of 216 mm, and overall width (W) of 291.8 mm. The front fillet of the body has a radius of 75 mm. The spoiler itself has an inclination of 5° from the horizontal line. The total length of the spoiler before 7.5 mm of fillet was applied is 50 mm.

A Computational Fluid Dynamics (CFD) simulation coupled with a continuous adjoint-based optimisation [29]–[31] is employed in this study. After creating the geometry, Pointwise meshing software was used to mesh the computational domain. The total length of the computational domain is $8L$, the total height of the computational domain is $5H$, and the total width is $5W$. The geometry itself is positioned after 2L from the inlet face. The uniform freestream velocity U_∞ of 10 m/s was set in x direction with the lower face acting as a moving ground and was assigned to have velocity as the same as freestream velocity, with the given kinematic viscosity ν of $1.5\text{x}10^{-5}$ resulting to Reynolds number $5.22\text{x}10^{5}$. This Reynolds number was used based on the model length L during the optimisation. An open-source CFD solver, OpenFOAM was used for the solver. This Reynolds number was chosen considering the computational cost and the optimisation. The outlet face was set as zero *inletOutlet* boundary condition, and the remaining walls (both sides and the top) of the virtual wind tunnel were set to slip wall. The unstructured mesh was utilised by applying anisotropic meshing close to the body wall and refinement zone at the rear end of the body, as depicted in **Figure 3**. The smallest cell has

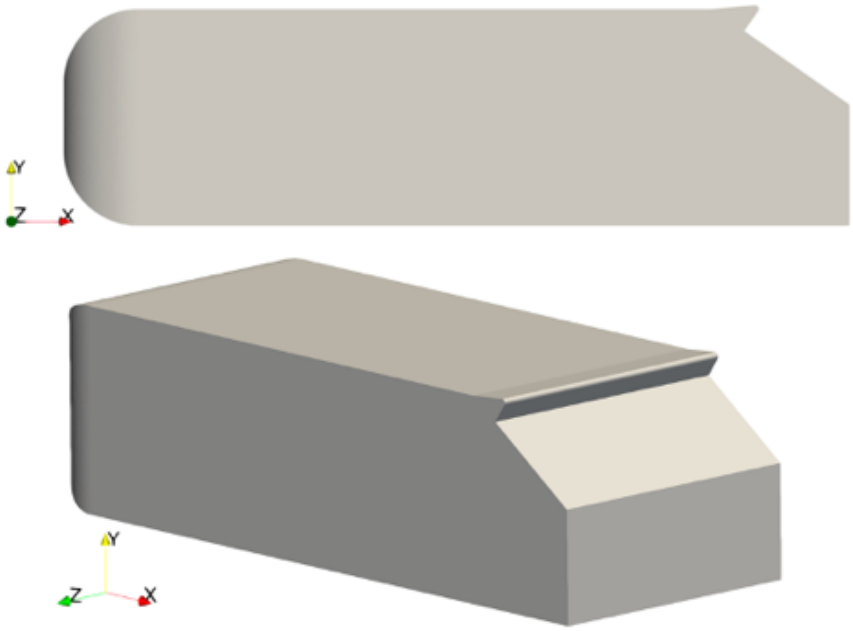

Figure 1. Ahmed Body Fitted with Spoiler Geometry.

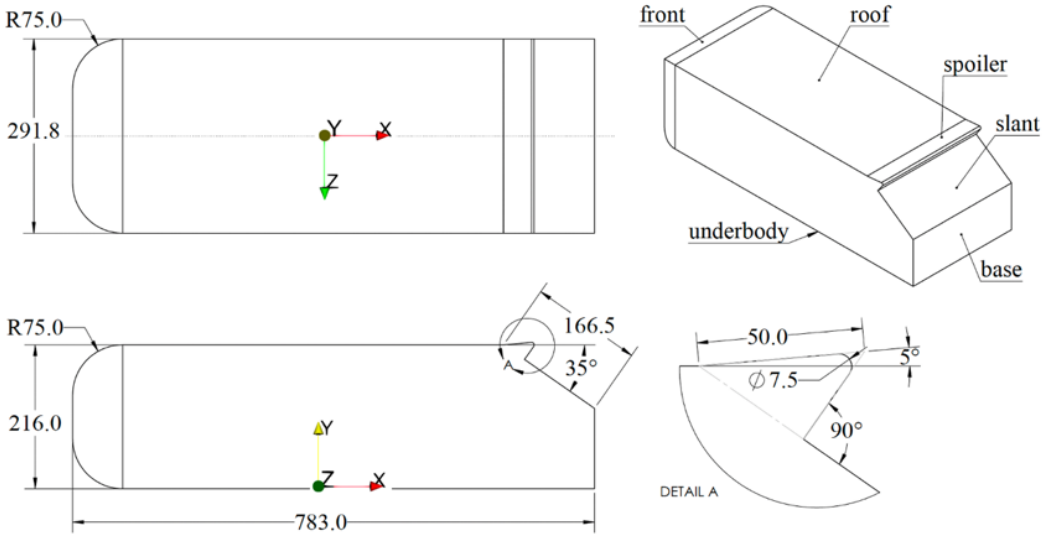

Figure 2. Model Dimension

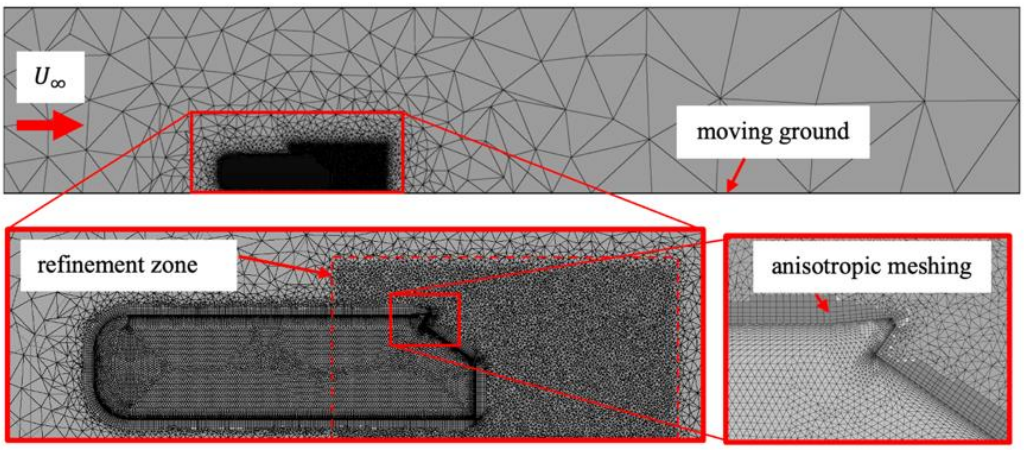

Figure 3. Generated Mesh with 3.8 million cells

the size of 0.02 mm and apply the growth rate of 1.2. Anisotropic layers were also applied to grow with maximum number of layers of 20. The *y+* value was targeted to about 30 and wall functions were applied at the wall of the model. After performing the mesh studies, the mesh used in this study employs the total number of cells generated is 3.8 million cells. The mesh in the area of the spoiler was set to be more refined, giving more dense surface mesh to ensure the smoothness of the spoiler region during the grid morphing and due to displacement of the optimisation.

3. Baseline Experimental Measurement

The experimental measurement of Ahmed body fitted by a rear spoiler was conducted by Cheng et al. [12]. The inflow air velocity was set so that it leads to a Reynolds number of 2.7×10^6 based on the model length. In order to validate the present simulation, the present simulation was also compared to the same setting with this Reynolds number. A computational fluid dynamic simulation was carried out to be compared to the experimental measurement. The present simulation also compared the pressure coefficient measurement at different measurement points indicated in the experiments. Several measurement point positions were introduced together with the point coordinates at which the values are measured (**Figure 4**). Three measurements positions were chosen from the rear end of the model roof, (1-3), two locations at the slant region (5 and 6), three at the base region (7-9) and three other points at the rear end of the underbody (10-12). All of those points are located at the symmetry plane of the Ahmed body model. **Figure 5** compares the resulting pressure coefficient of the present simulation and the experiment. The measurement results for both

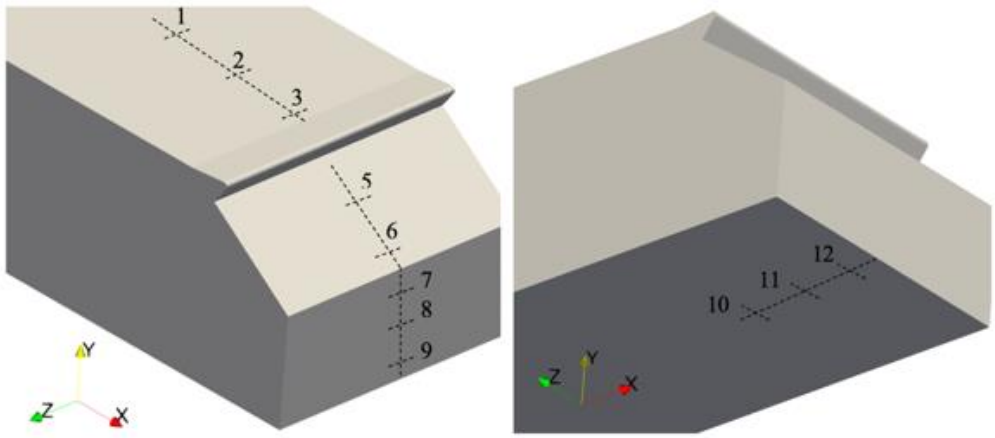

Measurement positions	1	2	3	-	5	6	7	8	9	10	11	12
x	-375	-295	-215	-	-92.19	-20.11	0	0	0	-21	-116.77	-215
y	338	338	338	-	325.69	275.22	165	125	65	50	50	50
z	0	0	0	-	0	0	0	0	0	0	0	0

Figure 4. Coordinate and locations of the measurement position in the experiment (reproduction from Ref [12]).

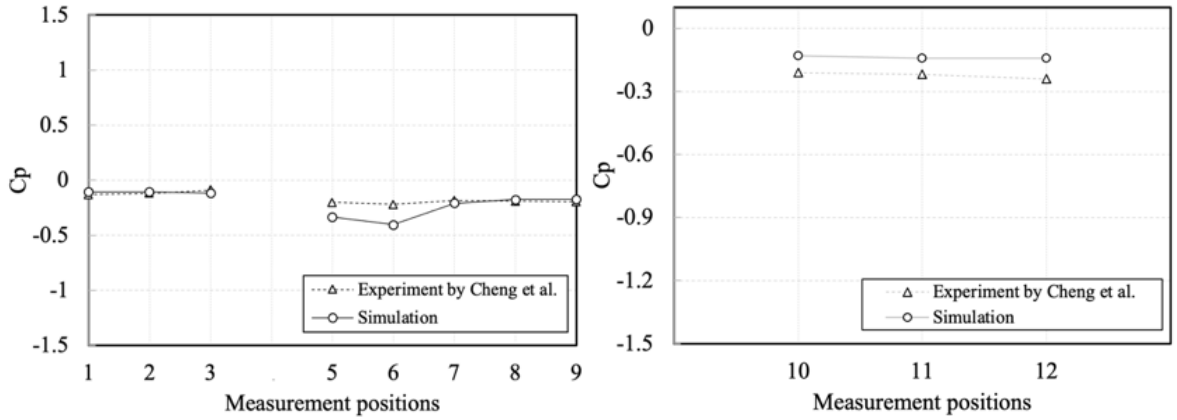

Figure 5. Comparison of the resulting pressure coefficient at the roof location (left) and underbody (right) between the present simulation and the experimental data.

experimental and simulation are relatively small differences except for the measurement at the slant location. However, the differences are still in an acceptable range. It is noticed in the present studies that there are relatively higher results differences in points 5 and 6, which are the points in the area of the slant, compared to the experimental results. It is suspected that the slant region is the area in which the recirculating region, lower pressure and unstable flow occur leading to possible higher discrepancies in the measurement. This condition might lead to higher differences between the present simulation and the experiment measurements. Additionally, some differences also occur at the measurement positions at the under body. The removal of the stilt in the simulation model affects these differences.

4. Continuous Adjoint Formulation and Scheme

The general mathematical explanation of continuous adjoint formulation for external aerodynamics implemented in OpenFOAM is discussed since this study mainly uses continuous adjoint, which have been developed and used by Ref. [29], [30], [32] which is chosen for the present optimisation algorithm, apart from another approach of the adjoint, such as discrete formulation [1], [31], [33] which is not covered in this study. This section only covers the general explanation of the adjoint formulation. More detailed about the adjoint equation derivation, boundary conditions, and solution method employed is also described in Ref. [29], [30], [32], which are applied also in this study.

The governing equation, which in this case is also called the primal equations, is the implementation of the steady-state Reynolds-Average Navier Stokes Equation (RANS) equation for incompressible flow (Eq. (1)-Eq. (3))

$$R^p = -\frac{\partial_{vi}}{\partial_{xi}} + 0 \quad (1)$$

$$R_i^v = v_j \frac{\partial v_i}{\partial x_j} + \frac{\partial p}{\partial x_j} - \frac{\partial}{\partial x_j}\left[(v + v_t)\left(\frac{\partial v_i}{\partial x_j} + \frac{\partial v_j}{\partial x_i}\right)\right] = 0 \quad (2)$$

$$R_i^z = convection + diffusion + disipation = 0 \quad (3)$$

where ν_i are the primal velocity components, p is the primal static pressure ν and ν_t are the kinematic and turbulent kinematic viscosity. R_i^z is any turbulence model applied with z_i denotes as multicomponent turbulence vector.

The formulation of the adjoint problem starts by defining the objective function F, which is expressed as follows Eq. (4) and Eq. (5).

$$F = \int_S F_s \, dS + \int_\Omega F_\Omega d\Omega \quad (4)$$

where the F is the augmented by the state equation, of R^p and R_i^v.

$$F_{aug} = F + \int_\Omega q R^p d\Omega + \int_\Omega u_i R_i^v d\Omega \quad (5)$$

In this case q and u_i are the adjoint variables, which are interpreted as adjoint pressure and adjoint velocity since they enter the solution algorithm. Frozen turbulence assumption is used in which derivation of the turbulence kinematic viscosity, v_t, is assumed constant when the design variables alter during the optimisation. Justification of complexity reduction becomes the main concern even if this might affect the sensitivity accuracy [31].

After performing differentiation of the augmented cost function, F_{aug}, yields the adjoint equations for incompressible flow with frozen turbulence (Eq. (6) and Eq. (7)).

As it is in the primal equation, the adjoint equation has similarities in having convection, diffusion, a gradient of pressure and source term. However, there is an additional term $u_j \frac{\partial \nu_j}{\partial x_i}$, in the adjoint momentum equation, which refers to adjoint transpose convection (ATC) [31].

A surface sensitivities of the objective function with respect to the movement of the normal direction of the surface nodes, the design variables, is calculated by the following expression (Eq. (8)).

The surface sensitivities are utilised as the input for the deformation of the surface and the computational domain. For the case of multi-point optimisation in this study, the weighted objective cost function F_t giving the weight in each objective was applied [23] as follows, where w_D and w_L correspond to weight value for both drag and lift respectively (Eq. (9)). The present study employed the Spalart-Allmaras [34] turbulence model, which the further explanation to the application to the adjoint model can be further studied in Ref. [30].

The complete derivation of the formulation can be further studied in Ref [23], [35], with some application has also been performed for the similar approach [29].

The multi-objective optimisation in this study aims to reduce the drag and reduce the lift (increase downforce). During the optimisation process, each of the objective functions was assigned with the appropriate weight function in Eq. (5) and Eq. (6). The free stream velocity is a 0° headwind. The surface of the spoiler is allowed to move only in x and y directions which will be further explained in the next section. The optimisation problem statement is in **Table 1**.

$$R_\Omega^q = \frac{\partial u_i}{\partial x_i} - \frac{\partial F}{\partial p} = 0 \quad (6)$$

$$R_{i\Omega}^u = -\nu_j \frac{\partial u_i}{\partial x_j} + u_j \frac{\partial \nu_j}{\partial x_i} + \frac{\partial q}{\partial x_j} - \frac{\partial}{\partial x_j}\left[(\nu + \nu_t)\left(\frac{\partial u_i}{\partial x_j} + \frac{\partial u_j}{\partial x_i}\right)\right] + \frac{\partial F}{\partial \nu_i} = 0 \quad (7)$$

$$\frac{\delta F_{aug}}{\delta b} = -\int_{S_w}\left[(\nu + \nu_t)\left(\frac{\partial u_i}{\partial x_j} + \frac{\partial u_j}{\partial x_i}\right) - q n_i\right]\frac{\partial \nu_j}{\partial x_k}\frac{\partial x_k}{\partial b_m} dS \quad (8)$$

$$F_t = w_D C_D^0 + w_L C_L^0 \quad (9)$$

Table 1. Optimisation problem statement

Category	Function/Variables	Explanation
Minimise	Drag Coefficient C_D Lift Coefficient C_L	Each of the objective function weight is assigned
With respect to	Headwind 0°	Constant freestream direction
Subject to	Constrained in Z	Spanwise movement of control points (z) is constrained

Each of the generated mesh in pre-processor steps will be solved based on the governing equations coupled with the adjoint equation for the optimisation. The complete flowchart of the solver can be seen in **Figure 6**.

After defining the objectives, specifying the design variables, constraints and determining the fluid flow and boundary condition, the primal equation was solved. The further explanation about design variables and constraints is explained in the next section. In this case, the use of incompressible Reylonds-Averaged Navier Stokes (RANS) equation for steady-state turbulence flow using a native OpenFOAM solver (*simpleFoam*) was implemented. The solver then computed the objective functions, quantifying the performance of the shape calculated. Since the proposed research aimed at multi-objective optimisation, there was a need to set the appropriate weight for each objective as explained in the previous section. Following that, the solver

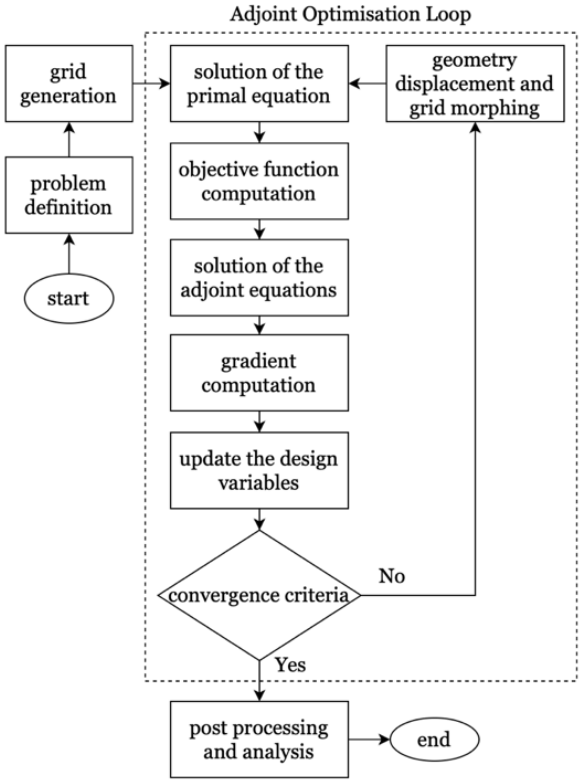

Figure 6. Continuous adjoint flowchart

will solve the turbulence model partial differential equation(s). In this case, since high-Re is applied, adjoint wall functions with the Spalart-Allmaras turbulence model were also introduced [30].

After the flow equation and adjoint formulation are calculated, the computation of the gradient of the defined objective functions(s) is carried out. At this stage, the sensitivity derivative (SD) formulations are utilised. Updating the design variables by utilising the previously calculated sensitivity derivatives will be the next step. Convergence study for adjoint solutions will be analysed to ensure the optimisation can reach a global optimum solution during the optimisation process. Moreover, the trade-off between multi-objective cases will also be explored, considering the potential conflicting objective functions. If the convergence criteria are not met, the optimisation will start the new loop, performing geometry displacement and grid morphing, and updating the vehicle shape is then performed based on the calculated design variables. This new geometry is then used for starting the new optimisation cycles. To update the mesh, the volumetric B-splines [36] tool is used to update both the geometry and the internal grid nodes.

5. Sensitivity Maps and Control Points

Before running the adjoint optimisation loop, the sensitivity derivatives of the two objectives function concerning the normal displacement of the surface of the model, in this case the spoiler needs to be computed. It results in a sensitivity map which tells the changes of the normal displacement of the surface of the spoiler can affect the drag and lift of the vehicle model. **Figure 7** shows the results of how sensitive the changes in the surface of the model to the reduction of the drag is, and **Figure 8** depicts the same case for the lift. The drag sensitivity map implies that there are two major areas that should draw the designer's attention to reduce vehicle drag. Those are the area of the spoiler, indicated by the red colour, and the rear end of the model, including the area

of the end of the underbody. The positive value (red colour) indicates that pulling out the surface will reduce the drag of the vehicle. The opposite effect applies to the blue area of the model. In other words, by pulling the surface out of the area around the spoiler to some points, the vehicle's drag will be reduced in the area of the underbody. Attention also needs to be given to the surface at the trailing edge of the model on the underbody. There is a significantly huge area of negative value based on the sensitivity maps (blue colour). This also means that pushing this blue area will achieve the objective function, i.e reducing the drag.

Figure 8 explains the possible regions that have the potential to be changed to achieve lift reduction. It shows that the trailing edge of the front fillet, upper part of the spoiler, trailing edge of the underbody and rear end of both side parts of the model are sensitive to the model lift. It is realised that a conflicting possible solution occurs at this stage. The region of the spoiler and the rear end of the underbody both significantly affect the objective function changes if the surface in that area is deformed. Therefore, multi-objective optimisation in this study is required to be carried out, discussing the possible solution to address the mentioned problem.

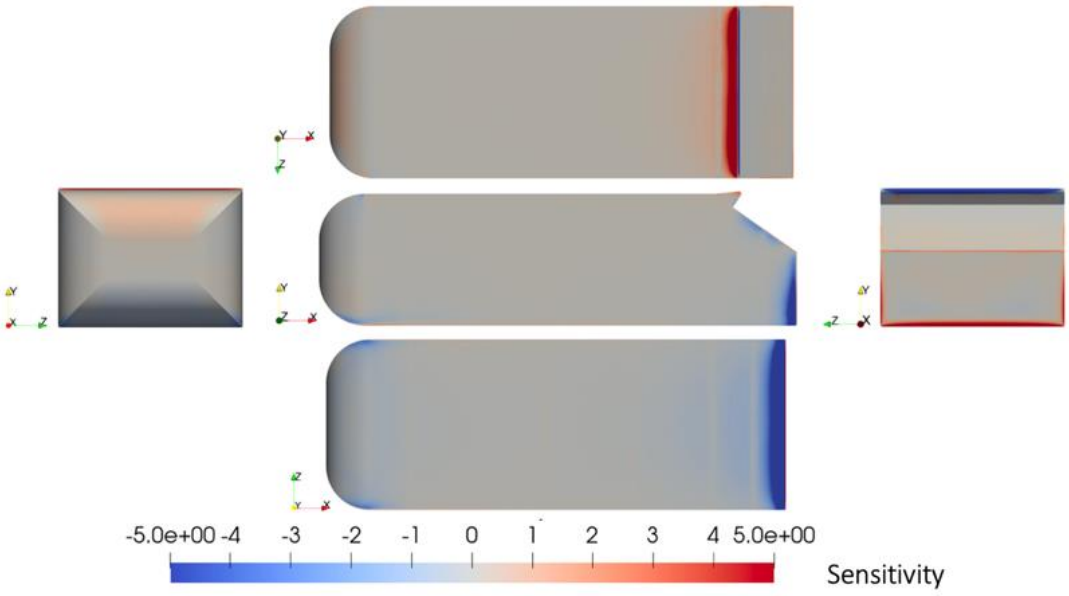

Figure 7. Drag Sensitivity Maps.

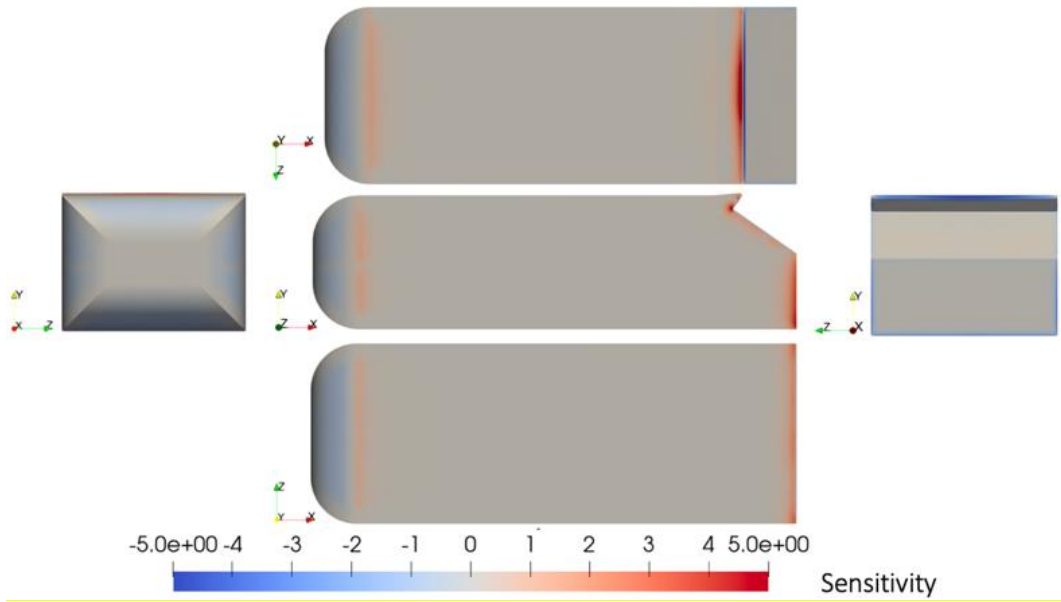

Figure 8. Lift Sensitivity Maps

Considering the computational cost, time, and resources, this research is limited to the optimisation of the spoiler region of the body. Guided by the results of the sensitivity maps due to the drag and the lift, the region intended to be optimised is defined by a morphing box with 8x6x15 control points to parameterise the spoiler shape (**Figure 9**). The outermost of the control point in x, y, and z directions is kept constant, which is indicated by the blue colour. The remaining control points, the ones with red colour, are allowed to vary during the optimisation. The moving control point are constrained in z direction, allowing them to move only in x and y direction to ensure that the deformed shape does not exceed both sides of the body. The symmetrical constraint between left and right side of the vehicle model is achieved by mirroring one side of the resulting optimisation of the model. Considering that, there are 624 design variables to control the movement of the spoiler shape. In this case, a volumetric B-Splines is used to parameterise the grid displacement during the mesh morphing considering their flexibility, smoothness, local control, and parametric nature. This parameterisation and grid displacement using this method can be further studies in Ref [23].

6. Result and Discussion

By setting the appropriate value of objective weight defined in Eq. 5 and 6, different points of the front of non-dominated solutions can be calculated, proposing different solutions of conflicting objectives function of the optimisation. Five different values of weight function for each objective were proposed and it yielded in Pareto front [37], [38] depicted in **Figure 10**. The graph shows the convergence history of each simulation starting from the baseline (Bs) point indicated by the green colour in the objective space. Each solution converges to the point of optimised results resulting in the pareto front solution for each defined objective weight, presented in the red colour for each optimisation. A steepest descent [39] method was used to update the design variables in each optimisation loop. The total optimisation cycle for all proposed optimisation solutions is 44 optimisation cycles. Each cycle consists of the calculation of the primal governing equation, and two adjoint solution for drag and lift. In total, the simulation run is equivalent to 132 flow solutions. The simulation was carried out in an Intel Processor of a High-Performance Computer with 32 cores running in parallel. Each of the optimisation cycles requires 1.72 hours, leading to about 75.68 hours of simulation, or about 3.15 days. Similar method has also originally been used by Papoutsis-Kiachagias et al. [23].

Figure 11 compares the resulting geometries and the baseline geometry of the optimisation. Each solution applies a different value of objective weight, as it is presented in **Figure 10**. The first optimisation (Opt1), applying the drag weight of 6 and lift weight of 0.1, is able to reduce the drag by 14 normalised values of $C_D/C_{D,0}$. However, the downforce (negative lift) decreases by more than five folds as it is compared to the lift value of the baseline geometry. The moderate proposed solution (Opt4), which has a drag weight value of 1 and lift objective weight value of 0.2, results in drag reduction by about 12 values of $C_D/C_{D,0}$, while the downforce increases to nearly three

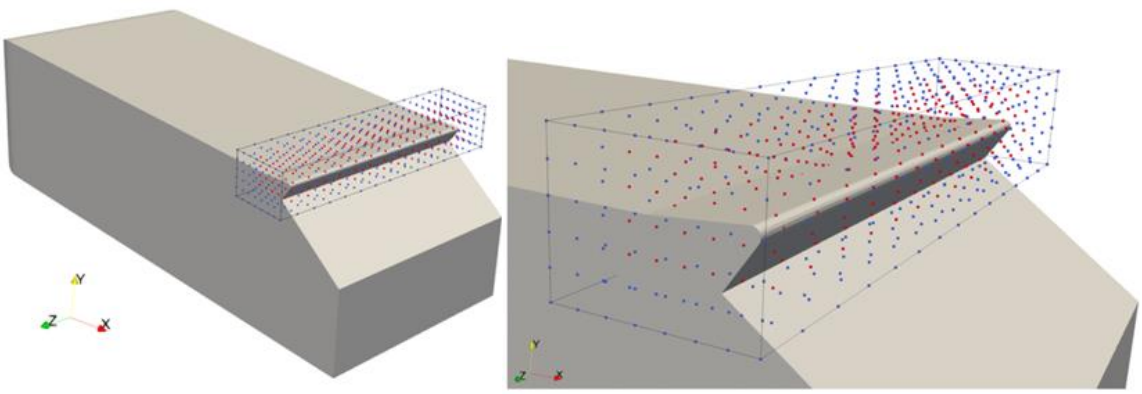

Figure 9. Control Points around the Rear Spoiler.

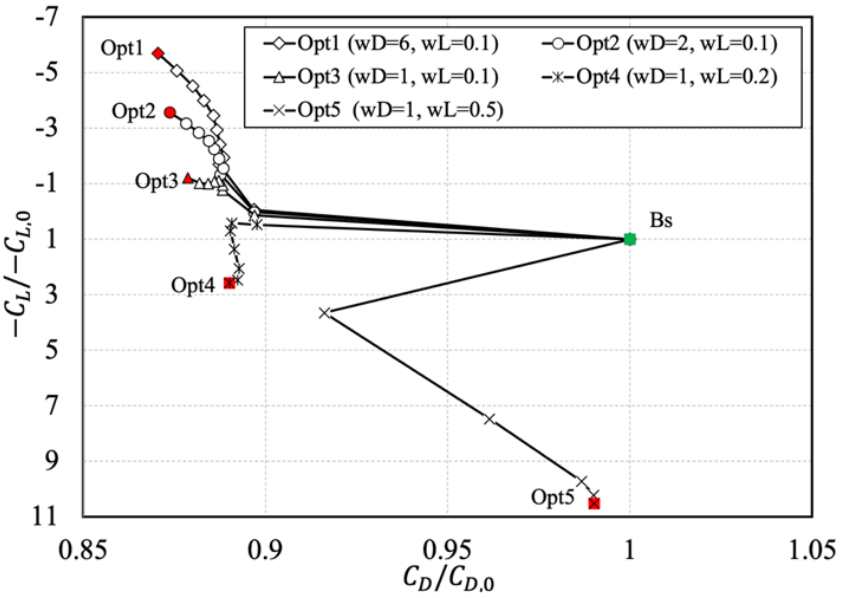

Figure 10. Pareto front and convergence history of optimisation. The values are normalised by the baseline drag and lift values.

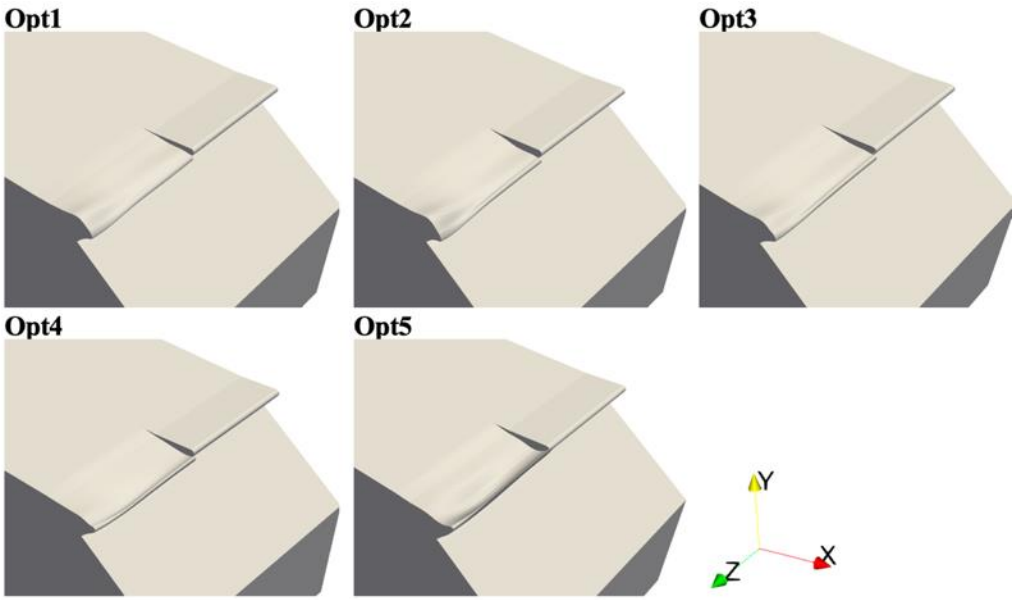

Figure 11. Baseline geometry and optimized geometries resulting from different weigh values.

times as the baseline (Bs) value. However, Opt5, applying the drag weight objective value of 1 and lift value of 0.5, can achieve the highest downforce among all solutions, while the drag has a slight decrease. The proposed solution shows the trade-off between the two conflicting objectives, giving a family of design solutions considering both the resulting value of drag and the downforce of the body. Assigning the weighted value of the objective function is the most common method used for multi-objective optimisation cases [37].

As the result of grid morphing during the optimisation, the surface of the spoiler deforms based on the sensitivity derivatives calculated by the adjoint algorithm to meet the objective function. This deformation can be seen in **Figure 12**, comparing the optimisation results of Opt1, Opt3, and Opt5, as the representation of the two extreme solutions and the one in the middle. Giving the $w_D = 6$ and $w_L = 0.1$ (Opt1) solution can achieve a considerable drag reduction while the resulting lift is higher than the baseline geometry. The surface deformation is rather deflecting the airflow, lowering the direction to energise the base pressure. Hence, the drag will decrease. The results show that the deformation is

not uniformly distributed along the spoiler. It has a higher displacement (by pushing down the surface) at both the left and right sides of the spoiler, letting the middle spoiler be higher than the other areas. The effects of the resulting base velocity are depicted in **Figure 13** to **Figure 17**, in terms of normalised velocity contour at the symmetry plane and some locations in the base. It can be observed that Opt1 results in the lower deflection of the air flowing through the spoiler if it is observed from the side. This solution also results in a smaller region of low velocity, which means the smaller region of low pressure, reducing drag.

Conversely, the application of the weight value of $w_D = 1$ and $w_L = 0.5$ (Opt5) results in a considerable increase in the downforce (minimise lift) while the reduction of the drag is slightly significant. The deformation of the surface can be seen in **Figure 12** bottom side. The optimised spoiler curving up at some points. When it is seen from the rear part of the body, the shape of the spoiler in the middle region is higher than the other parts. The top view of the body also shows that the deformation tends to make the spoiler have a concave shape at some points. It allows the airflow to be deflected up, and as a result it has more pressure on the area of the spoiler, generating downforce. However, the changes in the shape for Opt5 create a lower velocity region, making the low base pressure region increase, hence, the drag also increases. The differences in the low-velocity region can also be observed in **Figure 13**, which Opt5 solution generate a larger low-velocity region as it is compared to other solution and the baseline geometry.

Opt3, as the intermediate solution, gives the trade-off between downforce and drag force relatively a moderate solution. The drag force decreases, but the downforce also slightly decreases. However, the objective of reducing the drag can be met, but it instead generates more lift compared to the baseline geometry. The Opt4, instead, can achieve both drag reduction and generate more downforce as it is compared to the baseline results. At this point, it is clear that the application of different weights in each objective function yields different results in the drag and downforce value of each solution.

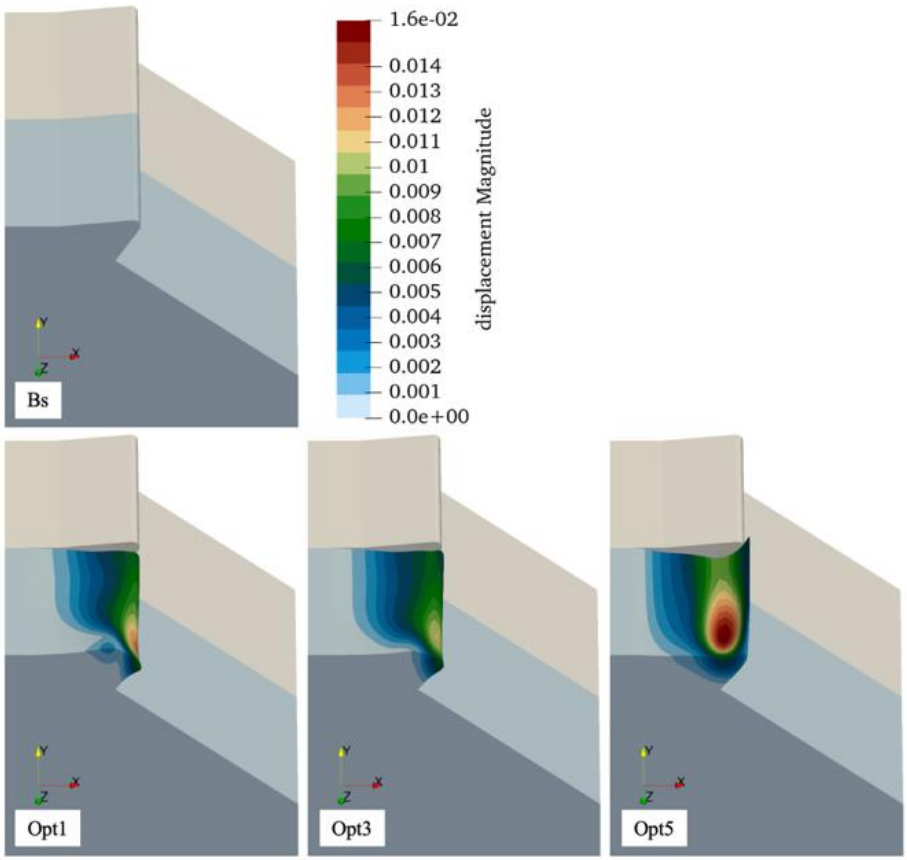

Figure 12. Cumulative magnitude displacement of optimised design Opt1, Opt3 and Opt5.

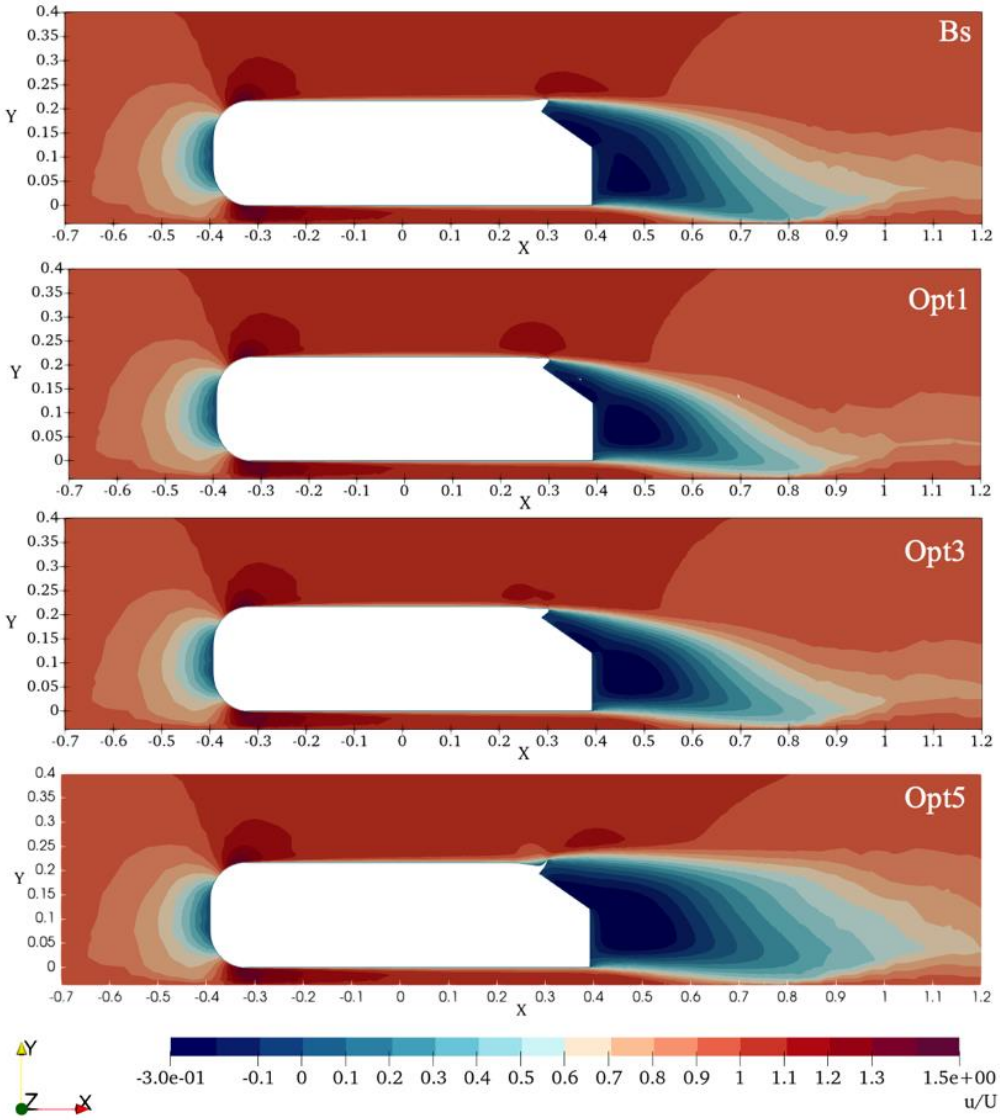

Figure 13. Normalised velocity u/U contour at the symmetry plane of the model comparing the baseline geometry (Bs) and proposed solution Opt1, Opt3 and Opt5.

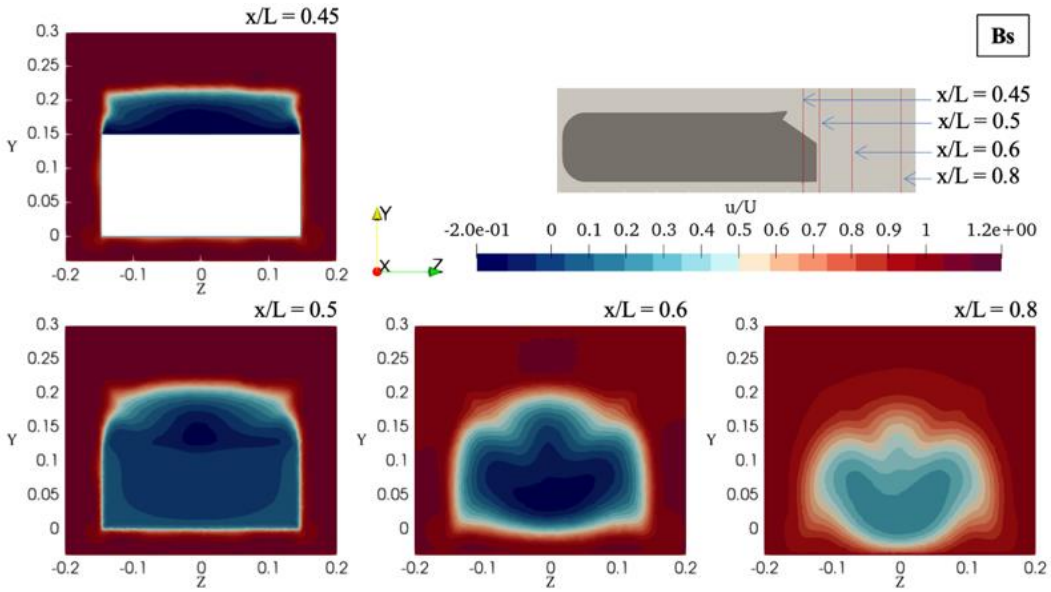

Figure 14. Normalised velocity contour at the base of the Baseline (Bs) model in three different locations .

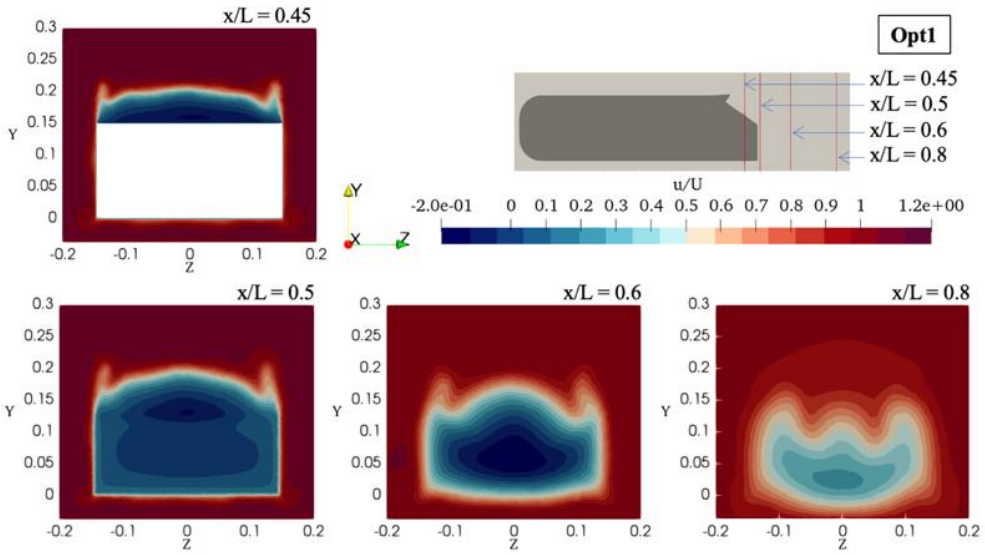

Figure 15. Normalised velocity contour at the base of the Opt1 model in three different locations.

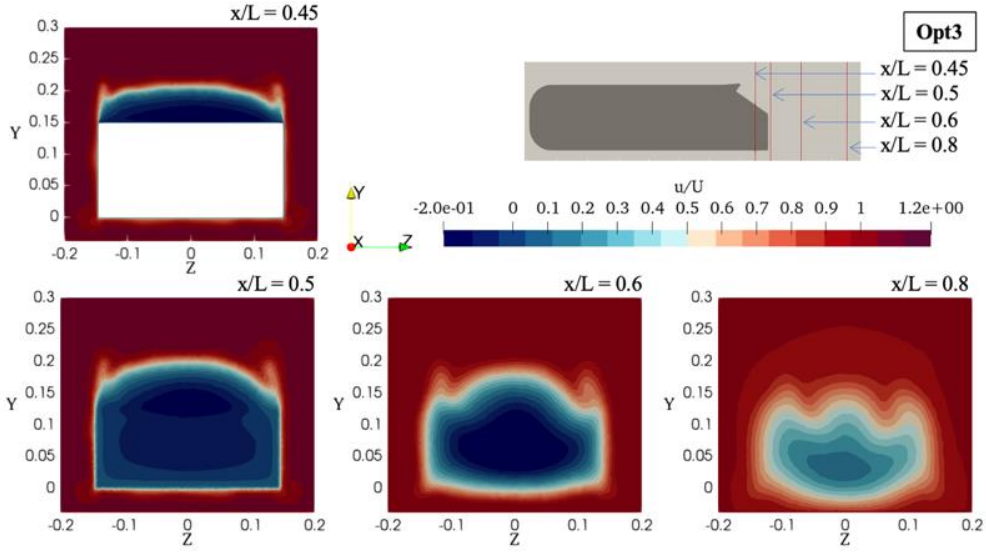

Figure 16. Normalised velocity contour at the base of the Opt3 model in three different locations.

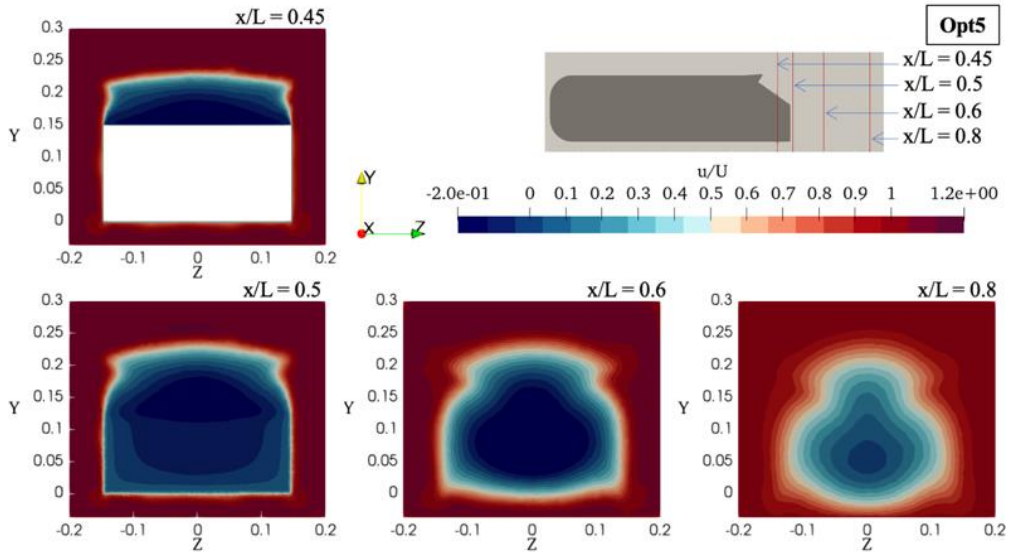

Figure 17. Normalised velocity contour at the base of the Opt5 model in three different locations.

Figure 18 shows the streamlines at the base by comparing the baseline and the other optimisation solutions. The plot was generated at the symmetry plane of the vehicle model. The baseline geometry generates one vortex core (VC) located at the rear slant of the vehicle. However, Opt1, Opt3, and Opt5 generate two huge vortex cores at the upper and lower part of the vehicle base. It is also shown that the change of the spoiler geometry changes the overall circulation length (CL) for each optimisation result. Generating more downforce by having the shape of Opt5 deflect the air so that it yields the longest circulation region at the rear of the vehicle model. Opt1, which yields the lowest drag, alters the location of the upper vortex core (VC1) to be lower than the baseline geometry. Among all the solutions, the baseline geometry has the shortest circulation length (CL).

The evaluation of the pressure coefficient has also become the interest of the investigation. The investigation of the pressure coefficient Cp comparison of the optimisation solution, simulation of the baseline geometry and the experimental measurement are compared in **Figure 19**, **Figure 20**, and **Figure 21**. It gives the explanation of the relative ratio of the differences between the local pressure, which in this case is along the upper part of the symmetry plane of the body, and the free-stream pressure. As expected, the changes in the spoiler shape mainly affect the pressure coefficient just prior to the spoiler, along the spoiler and the slant region of the body. The comparison of the experimental measurement shows that the calculation of this simulation is in good agreement. However, there is a slight difference in the results in the area of the slant, which is still in the range of the acceptable values. The measurement comparison at the base region agrees with the simulation and the experiment as well.

The optimisation solution in Opt1 affects the reduction of the pressure coefficient just before the optimised spoiler. It indicates that it generates a rather slower local velocity as compared to the freestream velocity, the value drops in negative value. It is hypothesised as the location where the separation starts to occur. However, the identification of the skin friction coefficient might be of interest to further identify this, which is beyond the scope of this article. Similar results can also be identified for the optimisation solution Opt3. It has been discussed in the previous section that Opt1 and Opt3 do not generate downforce, yet significantly reduce the drag of the body.

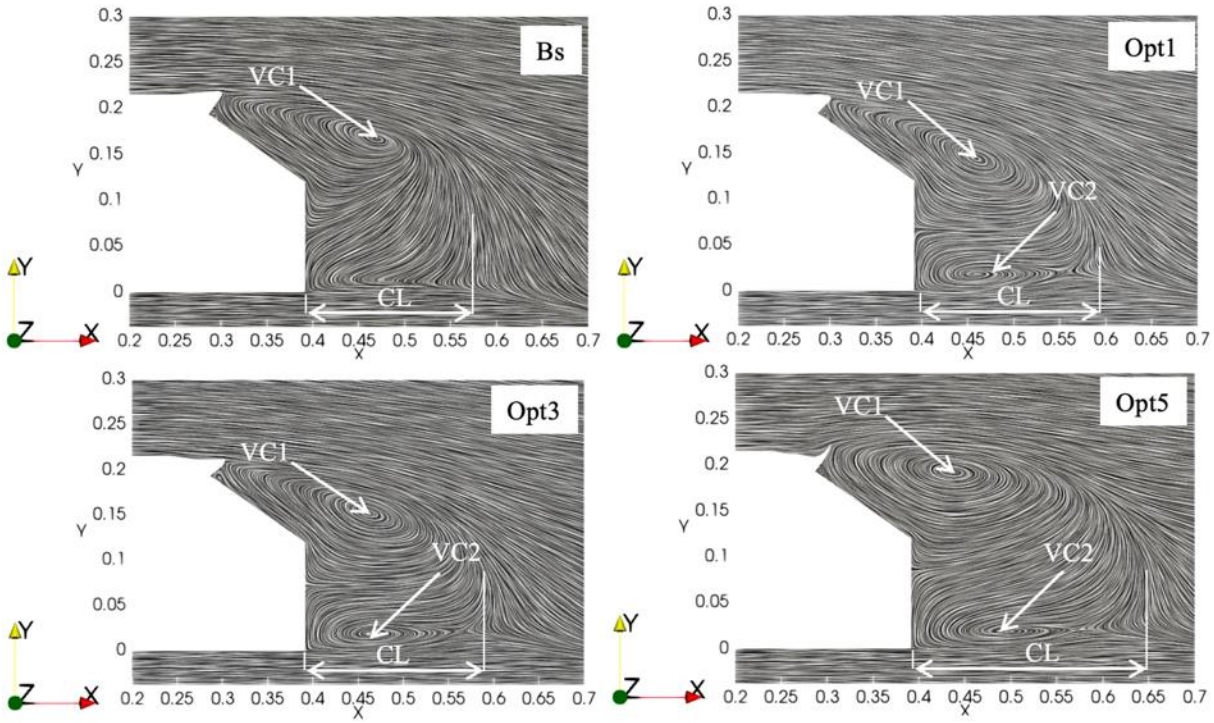

Figure 18. Streamlines contour at the base of the vehicle showing the vortex core (VC), and the overall circulation length (CL).

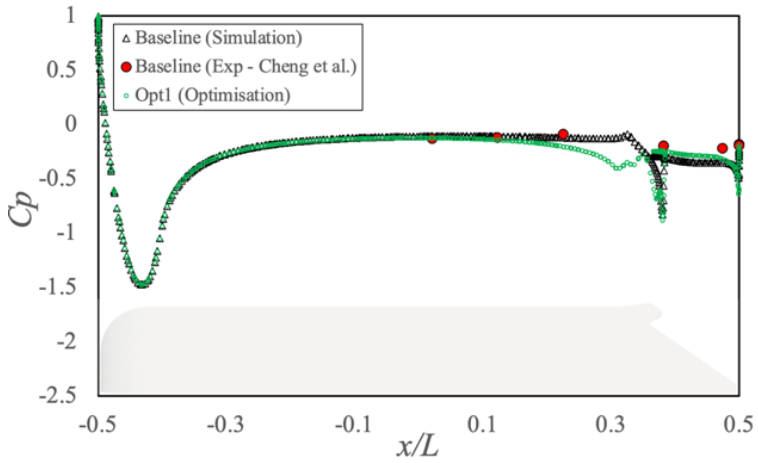

Figure 19. Pressure coefficient Cp comparison of the baseline geometry, experimental data and Opt1.

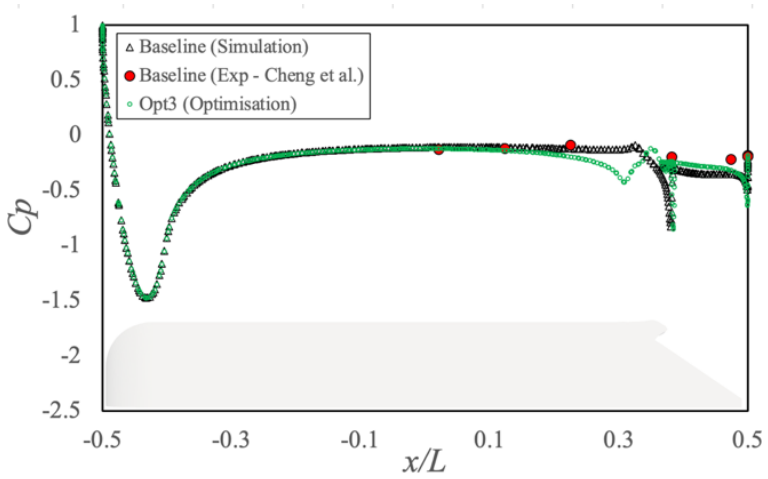

Figure 20. Pressure coefficient Cp comparison of the baseline geometry, experimental data and Opt3.

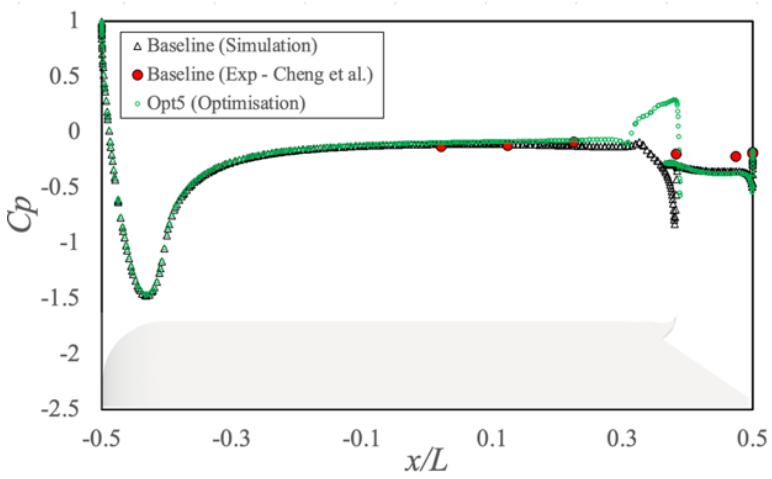

Figure 21. Pressure coefficient Cp comparison of the baseline geometry, experimental data and Opt5.

As contrast, the Opt5 generate a significantly higher pressure coefficient at the area of the spoiler since this optimisation solution deflects the airflow, increasing the local pressure at the region of the spoiler, hence the downforce greatly elevates. It can be observed that the local pressure coefficient at the spoiler rises more than zero value. The changes in the spoiler shape of this optimisation increase the surface air velocity due to its concave shape, growing the local pressure and increasing the downforce. However, the resulting drag of the body is sacrificed in this

solution. Giving the trade-off of the downforce outweighing the drag of the body as the result of the weighting value assigned to the objective function. For all the solutions (Opt1, Opt3, and Opt5), the resulting pressure coefficient drops as the flow leaves the spoiler, explaining the area of the flow separation occurs and starts to generate base pressure at the region of the base surface of the body.

The velocity profile over the slant region at the symmetry plane of the body can also be identified in **Figure 22** to **Figure 24**. The figures compare the resulting optimisation to the baseline normalised stream-wise velocity component at different locations at the slant region x/L. The main differences among the three optimisation solutions rely on the shift of normalise stream-wise velocity due to the change of the spoiler shape. When the optimisation reduces the drag (Opt1 and Opt3), the resulting streamwise velocity at the slant generates higher velocity than the baseline geometry. It energises the flow at the top of the slant region and reduces the drag. This result agrees with the previous graph regarding the velocity contour and more convincing results analysis. The optimisation solution generates higher downforce (Opt5), instead shifting the streamwise velocity forward compared to the baseline geometry. Moreover, the location where the local velocity reaches 99% of the free stream velocity, δ_{99}, also shows the differences. The optimisation solution to reduce the drag (Opt1, and Opt3) reach the δ_{99} at x/h both at below $x/h = 1.05$. However, optimising the spoiler to have greater downforce affects the location of the δ_{99} location, which becomes slightly higher than $y/h = 1.05$.

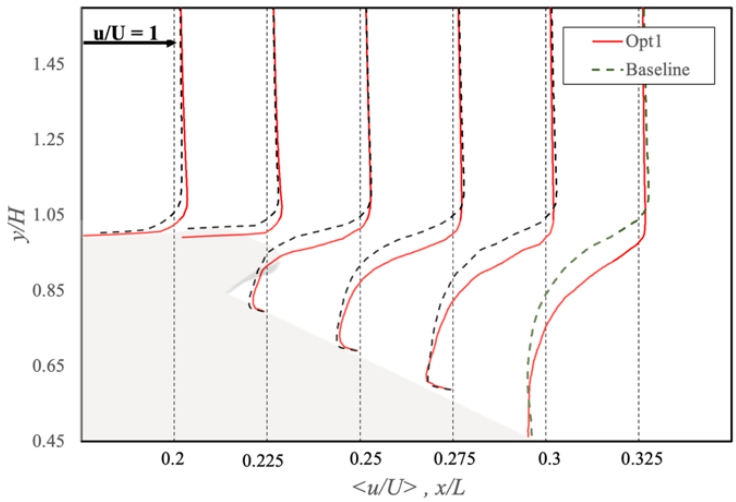

Figure 22. Normalised stream-wise velocity component/U profiles of the Bs and Opt1.

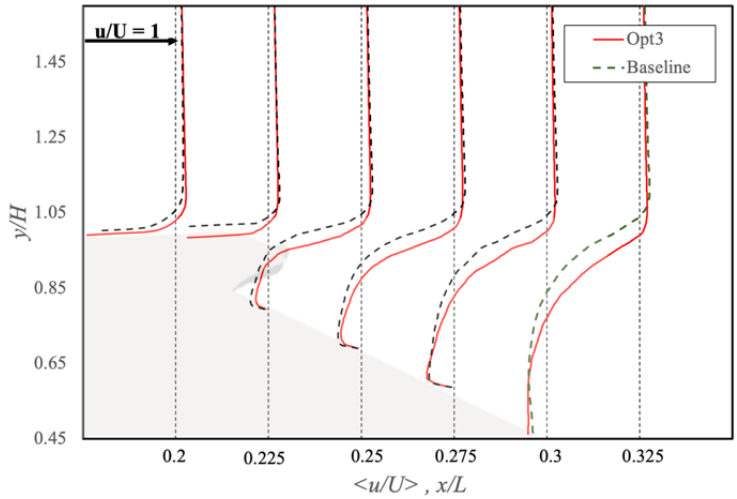

Figure 23. Normalised stream-wise velocity component/U profiles of the Bs and Opt3.

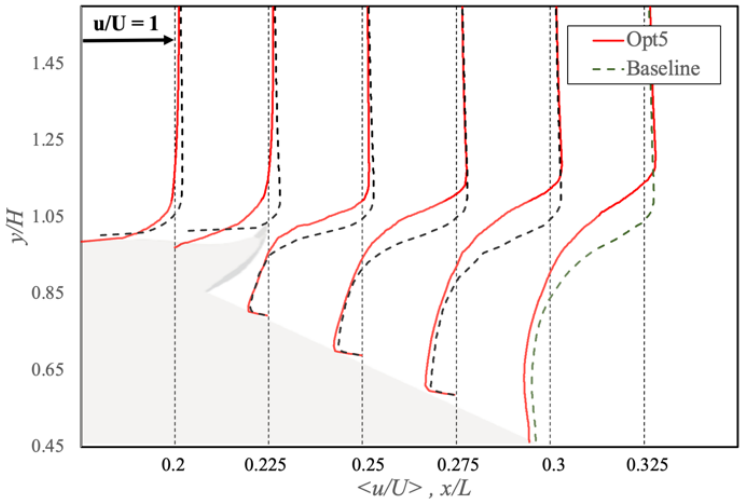

Figure 24. Normalised stream-wise velocity component/U profiles of the Bs and Opt5.

7. Conclusion

This study optimises the rear spoiler shape attached to a generic road vehicle model, Ahmed body. The conflicting objectives of reducing the drag and improving vehicle downforce were solved by using a continuous adjoint-based optimisation method with computational fluid dynamics simulation with an open-source solver OpenFOAM. The optimisation was carried out with respect to headwind conditions. The sensitivity maps investigation indicates that the region in the spoiler was the one region that need the designer's attention to optimise with respect to both drag and downforce. Therefore, the study was limited to modifying the spoiler's geometry to satisfy both conflicting objective functions. The movement of the surface during the optimisation was performed by means of volumetric B-Spline, which successfully performs well for mesh morphing. The optimisation can handle 624 design variables with a total calculation time for each optimisation of 1.72 hours with 32 cores processor running in parallel.

The multi-objective optimisation resulted in five different family of design, solving the trade-off between conflicting drag and downforce objectives. Assigning different weighted value of the objective function in the optimisation, the Pareto fronts of the non-dominated solution was obtained, having different results in drag reduction and downforce alteration of the spoiler's different shapes. Opt1 solution achieved a substantial reduction of drag force, but the vehicle model generated lift. On the other hand, the proposed solution Opt5 greatly increases vehicle downforce while slightly reducing the drag force. Detailed evaluations were also conducted by comparing the simulation results of the baseline geometry with the experiment and the results of this simulation are in good agreement with experimental results. Normalised velocity contours at the symmetry plane of the body and at the rear end of the vehicle model were also conducted. Opt1, which reduces the downforce, was able to energise the base pressure of the model, reducing the area of low velocity and increasing the base pressure, hence the drag reduces. However, this solution sacrifices the resulting downforce of the vehicle model. Instead, Opt5 increases surface pressure at the spoiler region and deflects the flow to generate local pressure, hence the downforce has a considerable increase. Some optimised design in between has their own trade-off between drag reduction and downforce increment. Analysis in terms of pressure coefficient also tells the behaviour of the model comparing the baseline and the modified spoiler shape. Analysis of normalised streamwise velocity component with respect to free-stream velocity was also investigated, explaining the flow behaviour that supports the results of the previous analysis. In general, giving more local pressure towards the vehicle model by deflecting up the rear spoiler can increase the downforce, which results in the larger region of the lower pressure at the base, resulting in a higher drag. Instead, drag reduction can be achieved by reducing the overall region of the lower pressure at the base by deflecting down the spoiler to some extent. However, this general finding is model-

dependent, since the aerodynamic behaviour depends of the flow history prior to the spoiler. A given freedom of the shape deformation results in a unique shape that manipulates the flow to achieve the objective of drag reduction or downforce generation of this multi-objective case. Further study following these results will be the re-evaluation of the obtained solution by implementing a high-fidelity simulation method to support the results of this work.

The adjoint-based optimisation method is a powerful tool for shape optimisation especially when there are many variables are involved. The mesh morphing is controlled by the calculation of the sensitivity derivatives of the objective function. When the case is having a headwind over the vehicle model, the flow over the vehicle model should be symmetry. However, when asymmetric flow is involved in the simulation, such as crosswind, the symmetry constraint is required to ensure the resulting shape deformation is symmetry during the optimisation. Moreover, it also needs to consider the manufacturability of the obtained shape for industrial application. When it is necessary to keep the deformed shape to be manufacturable, this study identify the most optimal suggested shape to achieve the objectives of the optimisation. That will also be a further potential study that will be conducted following this study.

Acknowledgements

This research was facilitated by the Computational Shared Facilities from the University of Manchester - UK. The funding was given by *Balai Pembiayaan Pendidikan Tinggi* (BPPT), *Beasiswa Pendidikan Indonesia* (BPI), together with *Lembaga Pengelola Dana Pendidikan* (LPDP) Indonesia with BPI number 202205080276.

Author's Declaration

Authors' contributions and responsibilities

The author made substantial contributions to the conception and design of the study. The authors took responsibility for data analysis, interpretation and discussion of results. The authors read and approved the final manuscript.

Funding

The research was funded by *Balai Pembiayaan Pendidikan Tinggi* (BPPT), *Beasiswa Pendidikan Indonesia* (BPI), together with *Lembaga Pengelola Dana Pendidikan* (LPDP) Indonesia with BPI number 202205080276.

Availability of data and materials

All data are available from the authors.

Competing interests

The authorsdeclare no competing interest.

Additional information

No additional information from the authors.

References

[1] L. Martinelli and A. Jameson, "Computational aerodynamics: solvers and shape optimization," *Journal of heat transfer*, vol. 135, no. 1, p. 11002, 2013, doi: 10.1115/1.4007649.

[2] S. N. Skinner and H. Zare-Behtash, "State-of-the-art in aerodynamic shape optimisation methods," *Applied Soft Computing*, vol. 62, pp. 933–962, 2018, doi: 10.1016/j.asoc.2017.09.030.

[3] C. Othmer, "Adjoint methods for car aerodynamics," *Journal of Mathematics in Industry*, vol. 4, no. 1, p. 6, 2014, doi: 10.1186/2190-5983-4-6.

[4] G. Gunadi, H. Sofyan, A. Yudianto, W. Setiawan, F. Julianto, and U. Aminudin, "On the options for bus aerodynamic profile optimization," in *AIP Conference Proceedings*, 2023, vol. 2671, no. 1, doi: 10.1063/5.0117392.

[5] A. Altaf, A. A. Omar, and W. Asrar, "Passive drag reduction of square back road vehicles," *Journal of Wind Engineering and Industrial Aerodynamics*, vol. 134, pp. 30–43, 2014, doi: 10.1016/j.jweia.2014.08.006.

[6] R. P. Putra, D. Yuvenda, M. Setyo, A. Andrizal, and M. Martias, "Body City Car Design of Two Passengers Capacity: A Numerical Simulation Study," *Automotive Experiences*, vol. 5, no. 2, pp. 163–172, Apr. 2022, doi: 10.31603/ae.6304.

[7] M. Szudarek, A. Piechna, and J. Piechna, "Feasibility Study of a Fan-Driven Device Generating Downforce for Road Cars," *Energies*, vol. 15, no. 15, p. 5549, 2022, doi: 10.3390/en15155549.

[8] Z. Arifin *et al.*, "Aerodynamic Characteristics of Ahmed Body with Inverted Airfoil Eppler 423 and Gurney Flap on Fastback Car," *Automotive Experiences*, vol. 5, no. 3, pp. 355–370, 2022, doi: 10.31603/ae.7067.

[9] C. Baker, F. Cheli, A. Orellano, N. Paradot, C. Proppe, and D. Rocchi, "Cross-wind effects

on road and rail vehicles," *Vehicle system dynamics*, vol. 47, no. 8, pp. 983–1022, 2009, doi: 10.1080/00423110903078794.

[10] A. Yudianto, W. Setiawan, F. Julianto, and U. Aminudin, "Aerodynamic study of vehicles in formation under crosswind," in *AIP Conference Proceedings*, 2023, vol. 2671, no. 1, doi: 10.1063/5.0114571.

[11] A. Yudianto, I. W. Adiyasa, and A. Yudantoko, "Aerodynamics of Bus Platooning under Crosswind," *Automotive Experiences*, vol. 4, no. 3, pp. 119–130, 2021.

[12] S.-Y. Cheng, K.-Y. Chin, and S. Mansor, "Experimental study of yaw angle effect on the aerodynamic characteristics of a road vehicle fitted with a rear spoiler," *Journal of Wind Engineering and Industrial Aerodynamics*, vol. 184, pp. 305–312, 2019, doi: 10.1016/j.jweia.2018.11.033.

[13] J.-F. Beaudoin and J.-L. Aider, "Drag and lift reduction of a 3D bluff body using flaps," *Experiments in fluids*, vol. 44, no. 4, pp. 491–501, 2008, doi: 10.1007/s00348-007-0392-1.

[14] J.-L. Aider, J.-F. Beaudoin, and J. E. Wesfreid, "Drag and lift reduction of a 3D bluff-body using active vortex generators," *Experiments in fluids*, vol. 48, pp. 771–789, 2010, doi: 10.1007/s00348-009-0770-y.

[15] G. Pujals, S. Depardon, and C. Cossu, "Drag reduction of a 3D bluff body using coherent streamwise streaks," *Experiments in fluids*, vol. 49, pp. 1085–1094, 2010, doi: 10.1007/s00348-010-0857-5.

[16] A. Thacker, S. Aubrun, A. Leroy, and P. Devinant, "Effects of suppressing the 3D separation on the rear slant on the flow structures around an Ahmed body," *Journal of Wind Engineering and Industrial Aerodynamics*, vol. 107, pp. 237–243, 2012, doi: 10.1016/j.jweia.2012.04.022.

[17] J. Howell, A. Sheppard, and A. Blakemore, "Aerodynamic drag reduction for a simple bluff body using base bleed," *SAE transactions*, pp. 1085–1091, 2003.

[18] W. Yi, W. SaGong, and H.-C. Choi, "Drag reduction of a three-dimensional car model using passive control device," in *Proceedings of the KSME Conference*, 2007, pp. 2868–2872.

[19] R. Lohner, O. Soto, and C. Yang, "An adjoint-based design methodology for CFD optimization problems," in *41st Aerospace Sciences Meeting and Exhibit*, 2003, p. 299, doi: 10.2514/6.2003-299.

[20] R. Askari, P. Shoureshi, M. R. Soltani, and A. Khajeh Fard, "Adjoint-Based Design Optimization of S-Shaped Intake Geometry," in *ASME International Mechanical Engineering Congress and Exposition*, 2017, vol. 58349, p. V001T03A008, doi: 10.1115/IMECE2017-71884.

[21] C. Hinterberger and M. Olesen, "Automatic geometry optimization of exhaust systems based on sensitivities computed by a continuous adjoint CFD method in OpenFOAM," SAE Technical Paper, 2010.

[22] E. de Villiers and C. Othmer, "Multi-objective adjoint optimization of intake port geometry," SAE Technical Paper, 2012.

[23] E. M. Papoutsis-Kiachagias, V. G. Asouti, K. C. Giannakoglou, K. Gkagkas, S. Shimokawa, and E. Itakura, "Multi-point aerodynamic shape optimization of cars based on continuous adjoint," *Structural and Multidisciplinary Optimization*, vol. 59, pp. 675–694, 2019, doi: 10.1007/s00158-018-2091-3.

[24] E. M. Papoutsis-Kiachagias, N. Magoulas, J. Mueller, C. Othmer, and K. C. Giannakoglou, "Noise reduction in car aerodynamics using a surrogate objective function and the continuous adjoint method with wall functions," *Computers & Fluids*, vol. 122, pp. 223–232, 2015, doi: 10.1016/j.compfluid.2015.09.002.

[25] A. Yudianto, U. Aminudin, W. Setiawan, and F. Julianto, "Aerodynamic investigation of misaligned four-vehicle platoon," in *AIP Conference Proceedings*, 2023, vol. 2671, no. 1, doi: 10.1063/5.0114577.

[26] A. Yudianto, H. Sofyan, and N. A. Fauzi, "Aerodynamic characteristics of overtaking bus under crosswind: CFD investigation," *CFD Letters*, vol. 14, no. 8, pp. 20–32, 2022, doi: 10.37934/cfdl.14.8.2032.

[27] A. Yudianto, M. Solikin, S. Sutiman, Z. Arifin, Iw. Adiyasa, and A. Yudantoko, "Aerodynamic investigation of extremely efficient vehicles under side wind conditions," *Revista Facultad de Ingeniería*

Universidad de Antioquia, no. 109, pp. 79–88, 2023, doi: 10.17533/udea.redin.20221107.

[28] S. R. Ahmed, G. Ramm, and G. Faltin, "Some salient features of the time-averaged ground vehicle wake," *SAE transactions*, pp. 473–503, 1984.

[29] E. M. Papoutsis-Kiachagias and K. C. Giannakoglou, "Continuous adjoint methods for turbulent flows, applied to shape and topology optimization: industrial applications," *Archives of Computational Methods in Engineering*, vol. 23, no. 2, pp. 255–299, 2016, doi: 10.1007/s11831-014-9141-9.

[30] A. Bueno-Orovio, C. Castro, F. Palacios, and E. Zuazua, "Continuous adjoint approach for the Spalart-Allmaras model in aerodynamic optimization," *AIAA journal*, vol. 50, no. 3, pp. 631–646, 2012, doi: 10.2514/1.J051307.

[31] S. Nadarajah and A. Jameson, "A comparison of the continuous and discrete adjoint approach to automatic aerodynamic optimization," in *38th Aerospace sciences meeting and exhibit*, 2000, p. 667, doi: 10.2514/6.2000-667.

[32] S. Thomas and O. Carsten, "Adjoint optimization for vehicle external aerodynamics," *International Journal of Automotive Engineering*, vol. 7, no. 1, pp. 1–7, 2016, doi: 10.20485/jsaeijae.7.1_1.

[33] P. He, C. A. Mader, J. R. R. A. Martins, and K. J. Maki, "An aerodynamic design optimization framework using a discrete adjoint approach with OpenFOAM," *Computers & Fluids*, vol. 168, pp. 285–303, 2018, doi: 10.1016/j.compfluid.2018.04.012.

[34] P. Spalart and S. Allmaras, "A one-equation turbulence model for aerodynamic flows," in *30th aerospace sciences meeting and exhibit*, 1992, p. 439.

[35] I. S. Kavvadias, E. M. Papoutsis-Kiachagias, and K. C. Giannakoglou, "On the proper treatment of grid sensitivities in continuous adjoint methods for shape optimization," *Journal of Computational Physics*, vol. 301, pp. 1–18, 2015, doi: 10.1016/j.jcp.2015.08.012.

[36] F. Massarwi and G. Elber, "A B-spline based framework for volumetric object modeling," *Computer-Aided Design*, vol. 78, pp. 36–47, 2016, doi: 10.1016/j.cad.2016.05.003.

[37] J. R. R. A. Martins and A. Ning, *Engineering design optimization*. Cambridge University Press, 2021.

[38] Y. Sawaragi, H. Nakayama, and T. Tanino, "Theory of Multiobjective Optimization. Elsevier," 1985.

[39] J. C. Meza, "Steepest descent," *Wiley Interdisciplinary Reviews: Computational Statistics*, vol. 2, no. 6, pp. 719–722, 2010.